Depinning Transition of Self-Propelled Particles

Arthur V. Straube[1, 2, *] and Felix Höfling[2, 1]

[1] *Zuse Institute Berlin, Takustraße 7, 14195 Berlin, Germany*

[2] *Freie Universität Berlin, Department of Mathematics and Computer Science, Arnimallee 6, 14195 Berlin, Germany*

Depinning transitions occur when a threshold force must be applied to drive an otherwise immobile system. For the depinning of colloidal particles from a corrugated landscape, we show how active noise due to self-propulsion impacts the nature of this transition, depending on the speed and the dimensionality d of rotational Brownian motion: the drift velocity exhibits the critical exponent $1/2$ for quickly reorienting particles, which changes to $d/2$ for slow ones; in between these limits, the drift varies superexponentially. Different giant diffusion phenomena emerge in the two regimes. Our predictions extend to systems with a saddle-node bifurcation in the presence of a bounded noise. Moreover, our findings suggest that nonlinear responses are a sensitive probe of nonequilibrium behavior in active matter.

A depinning transition occurs when a physical system is driven out of an immobile, localized state by an external force f such that, upon increasing the force above a critical value f_c, the system depins and starts to slide with a drift velocity v_D [1–3]. When approaching the transition from above, this response to the driving varies as a power law, $v_\mathrm{D} \sim (f - f_\mathrm{c})^\beta$, with a universal scaling exponent β. The phenomenon appears in a variety of contexts: it governs the onset of motion of fronts [4–6], contact lines [7], and domain walls [8–10], but also of vortices in superconductors [11–13] and magnetic skyrmions [14]. The depinning transition is fundamental for the phenomena of sliding friction and superlubricity [15–19], synchronization [20], and locking [21–26]. Colloidal systems have given exquisite insight into the depinning transition of individual particles [27–30], monolayers [31–34], and in glasses [35–37].

Unlike passive matter, active particles—motile microorganisms, artificial microswimmers, and active colloids—propel themselves and perform a directed motion, with the direction randomized as a function of time [38–42]. Experimental research in the field is fueled by the vision of microrobots performing specific transport tasks [43–45]; such particles move through structured channels, blood vessels, or surmount geometric constrictions [46]. More fundamentally, the inherently nonequilibrium nature of self-propulsion leads to a nontrivial interplay with a patterned substrate [42, 47–50], with impact on the macroscopic transport and inducing, e.g., directionality [51], negative mobility [52, 53], or superdiffusion [54]. One anticipates that self-propulsion also has significant ramifications on the depinning transition, which is an open issue.

In this work, we answer this basic question within the paradigm of the active Brownian particle (ABP) driven over a periodic landscape. The response is contrasted to that of a passive particle, whose drift velocity is known to exibit a power law with exponent $\beta = 1/2$ near depinning. We show that the activity modifies the nature of the transition, including a change of the exponent to some β', superexponential behavior, the emergence of another singular point, and an unbounded enhancement of the diffusivity in between. The new exponent $\beta' = d/2$ is sensitive to the dimensionality d of rotational Brownian motion.

Model. We use the framework of an ABP confined to a periodic potential energy landscape $U(\boldsymbol{r})$ and subjected to an external force $\boldsymbol{f}$ [Fig. 1(a)]. The position $\boldsymbol{r}$ and the orientation $\boldsymbol{u}$ of the ABP satisfy the Itō–Langevin equations [55, 56]:

$$\dot{\boldsymbol{r}}(t) = \mu_0[\boldsymbol{f} - \nabla U(\boldsymbol{r}(t))] + v_\mathrm{A}\boldsymbol{u}(t) + \boldsymbol{\xi}(t)\,, \tag{1}$$

$$\dot{\boldsymbol{u}}(t) = \boldsymbol{\omega}(t) \times \boldsymbol{u}(t) - \tau_\mathrm{R}^{-1}\boldsymbol{u}(t)\,, \tag{2}$$

where $v_\mathrm{A} \geqslant 0$ is the propulsion strength and μ_0 is the mobility of the free particle. The random linear and angular velocities, $\boldsymbol{\xi}$ and $\boldsymbol{\omega}$, respectively, are Gaussian white noise processes with zero means, $\langle\boldsymbol{\xi}(t)\rangle = 0$ and $\langle\boldsymbol{\omega}(t)\rangle = 0$, and covariances $\langle\boldsymbol{\xi}(t)\otimes\boldsymbol{\xi}(t')\rangle = 2D_0\mathbb{1}\delta(t-t')$ and $\langle\boldsymbol{\omega}(t)\otimes\boldsymbol{\omega}(t')\rangle = 2D_\mathrm{R}\mathbb{1}\delta(t-t')$. Here, D_0 and D_R are the translational and rotational diffusion constants, respectively. With $\tau_\mathrm{R}^{-1} = (d-1)D_\mathrm{R}$, Eq. (2) implies that $\boldsymbol{u}(t)$ performs an unbiased diffusion on the unit circle ($d = 2$) or unit sphere ($d = 3$) [56]. In the stationary limit, all directions of $\boldsymbol{u}$ are equally probable and the evolution of $\boldsymbol{u}(t)$ yields $\langle\boldsymbol{u}(t)\rangle = 0$ and $\langle\boldsymbol{u}(t)\cdot\boldsymbol{u}(t')\rangle = \exp(-|t-t'|/\tau_\mathrm{R})$; hence, τ_R is the persistence time of the orientation. In the following, we will mainly consider the case $d = 3$ because of its relevance for applications [48, 57–59].

As the potential, we employ the prototypical one-dimensional corrugated landscape [60] with a cosine shape: $U(\boldsymbol{r}) = U_\mathrm{L}(1 - \cos kx)$ with $x = \boldsymbol{r}\cdot\boldsymbol{e}_x$ and the unit vector $\boldsymbol{e}_x$ pointing perpendicular to the ripples; U_L is the amplitude of the landscape and k its wavenumber, equivalently, $\lambda = 2\pi/k$ its wavelength. Translational symmetry allows us to fix the direction of the force to $\boldsymbol{f} = f\boldsymbol{e}_x$ with $f \geqslant 0$. Focusing on the depinning singularity, we switch off the translational Brownian noise ($D_0 = 0$), which is known to mask the singular behavior at the critical point such that a rounded rather than sharp transition is observed [61–63]. With this, the

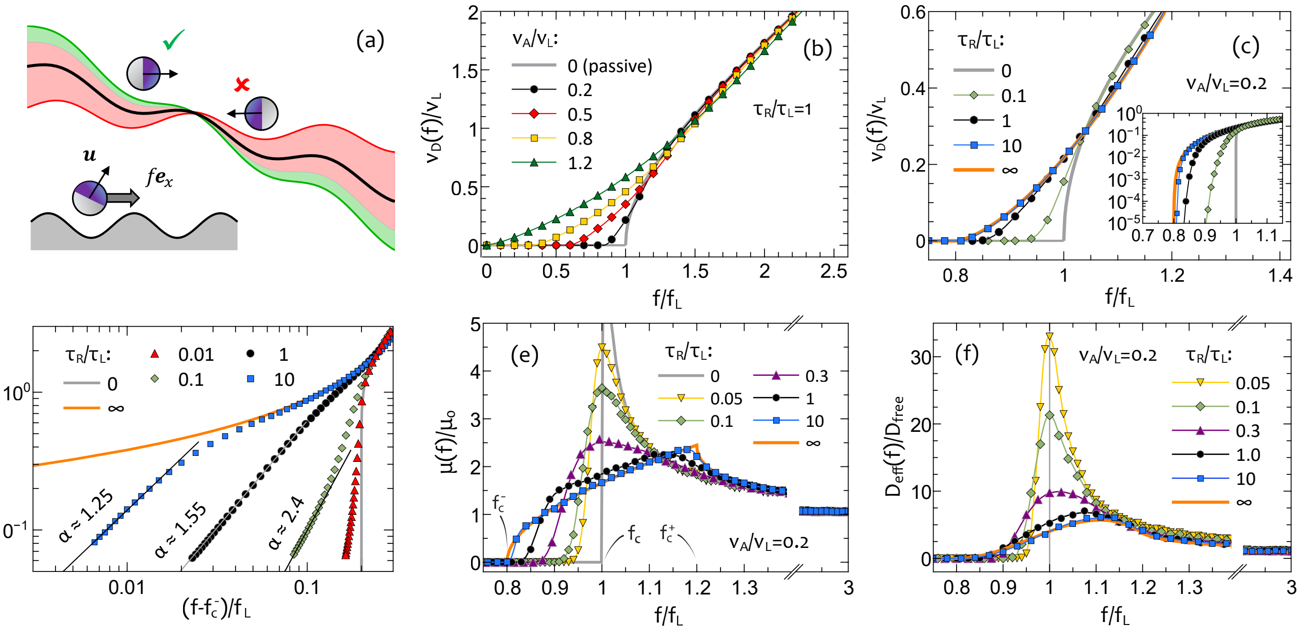

FIG. 1. Panel (a): Depinning of an active Janus particle from a corrugated potential landscape and subject to a driving force f (bottom) and the mapping to passive motion in a randomly tilted potential landscape (top). The tilt has a constant contribution $-fx$ (black line), which is increased (green line) or decreased (red line) depending on the orientation $\boldsymbol{u}(t)$. Panels (b),(c): Drift velocity $v_D(f)$ of the active particle with (b) fixed rotational persistence time $\tau_R = \tau_L$ but varying propulsion velocity v_A and (c) fixed $v_A = 0.2v_L$ but varying τ_R. In panel (b), the inset shows the same data as in the main panel on a logarithmic scale. Panel (d): high-precision data for $v_D(f)/v_L$ from the numerical solution of the Fokker–Planck equation, shown on an iterated logarithmic scale and corroborating the superexponential convergence of $v_D(f) \to 0$ as $f \downarrow f_c^-$ [Eq. (9)]. Panels (e),(f): Differential mobility $\mu(f) = \mathrm{d}v_D(f)/\mathrm{d}f$ and effective diffusion constant $D_{\mathrm{eff}}(f)$ as functions of the driving force f for fixed $v_A = 0.2v_L$ and varying τ_R. All panels: thin lines interpolate between stochastic simulation results (symbols); thick lines are analytic predictions for the limits of the hyper wobbler (gray, $\tau_R \to 0$) and the lazy wobbler (orange, $\tau_R \to \infty$).

model reduces to an Adler equation amended by an "active noise" $v_A u_x(t) = v_A \boldsymbol{u}(t) \cdot \boldsymbol{e}_x$:

$$\dot{x}(t) = \mu_0[f - f_L \sin(kx(t))] + v_A u_x(t)\,. \tag{3}$$

The characteristic force $f_L = U_L k$, the velocity $v_L = \mu_0 f_L$ and the timescale $\tau_L = \lambda/v_L$ serve us as a system of independent units. Regimes of different responses are distinguished by the relative strengths of the external driving f/f_L, the active propulsion v_A/v_L, and the rotational noise τ_R/τ_L. For the stochastic simulations, we combined Euler integration of Eq. (3) with a geometric scheme for Eq. (2) [56] and noise reduction [64]. The drift velocity was calculated from averaging over the driven stationary ensemble as $v_D(f) = \lim_{t\to\infty} \langle x(t)\rangle_f / t$; the variance yielded the dispersion coefficient or effective diffusion constant: $D_{\mathrm{eff}}(f) = \lim_{t\to\infty} \mathrm{Var}[x(t)]_f / 2t$.

The r.h.s. of Eq. (3) may also be viewed as originating from a tilted potential, $U(x) - [f + (v_A/\mu_0)u_x(t)]x$. Its barriers can only be crossed if $u_x > u_{x,c} = (v_L/v_A)(1 - f/f_L)$ [Fig. 1(a), green shading] and they act as a randomly rocking ratchet, rectifying the *a priori* unbiased self-propelled motion and thus facilitating transport.

Depinning transition. For passive motion, $v_A = 0$, the particle's response to the driving is governed by the dynamic system $\dot{x} = g(x, f)$ with $g(x, f) = \mu_0(f - f_L \sin kx)$, which exhibits a saddle-node bifurcation [65]. Two equilibria $x_*^{\pm} \in [0, \lambda)$, obeying $g(x_*, f) = 0$, exist for $f < f_c$ and disappear at the critical point $f_c = f_L$, which is determined by the additional requirement $\partial_x g(x_*, f_c) = 0$. Thus, the particle is pinned by the landscape for $f < f_L$ and remains immobile, $v_D(f) = 0$. For $f > f_L$, the particle slides with $v_D(f) = \lambda/\tau_1(f)$, where $\tau_1(f) = \int_0^\lambda g(x, f)^{-1}\,\mathrm{d}x$ is the time it takes the particle to travel one wavelength. With the present potential, one finds for the drift velocity of the passive particle:

$$v_D^{(p)}(f) = \mu_0 \sqrt{f^2 - f_L^2}\,, \qquad f > f_L, \tag{4}$$

which admits for the scaling form $v_D^{(p)}(f) = v_L s(f/f_L)$ with the rescaled force $y = f/f_L$ and the scaling function $s(y) = \sqrt{y^2 - 1}$ for $|y| > 1$ and $s(y) = 0$ otherwise. Expanding Eq. (4) close to the critical point, $f_c = f_L$, shows that $v_D^{(p)}(f)$ exhibits a square-root singularity,

$$v_D^{(p)}(f \downarrow f_c) \sim (f - f_c)^{\beta}, \quad \beta = 1/2. \tag{5}$$

For the self-propelled particle, $v_A > 0$, the force–velocity relationship obtained from the simulations shows progressively stronger deviations of $v_{\mathrm{D}}(f)$ from the square-root law (4) upon gradually increasing the propulsion strength v_{A} while fixing the orientational persistence time $\tau_{\mathrm{R}} = \tau_{\mathrm{L}}$ [Fig. 1(b)]. Conversely, changing τ_{R} at fixed $v_{\mathrm{A}} = 0.2 v_{\mathrm{L}}$ yields a similar picture [Fig. 1(c)]; the dependencies remain the same qualitatively when using other values of τ_{R} or v_{A}. Importantly, the ABP with $v_{\mathrm{A}} > 0$ and $\tau_{\mathrm{R}} > 0$ displays a nonzero drift also for $f < f_{\mathrm{c}}$. At first sight, this seems to resemble the rounding of the depinning transition caused by translational Brownian noise [61]. However, we will show that the effect of active propulsion on the transition is entirely different and cannot be mimicked by translational diffusion, $D_0 > 0$. In particular, a pinned state exists in the presence of self-propulsion for $f < f_{\mathrm{c}}^-$ with the new, shifted threshold $f_{\mathrm{c}}^- = f_{\mathrm{L}} - v_{\mathrm{A}}/\mu_0$ [66].

The existence of this activity-controlled critical force f_{c}^- is justified by the second observation: upon varying τ_{R} from 0 to ∞ at fixed ratio $v_{\mathrm{A}}/v_{\mathrm{L}} < 1$, the force–velocity curves interpolate monotonically between the analytical solutions for the "hyper wobbler" ($v_{\mathrm{A}} > 0$, $\tau_{\mathrm{R}} \to 0$) and the "lazy wobbler" ($\tau_{\mathrm{R}} \to \infty$, i.e., $D_{\mathrm{R}} \to 0$) [Fig. 1(c)]. The hyper wobbler is an ABP with a rapidly changing orientation such that τ_{R} is the smallest timescale of the problem, $\tau_{\mathrm{R}} \ll \tau_{\mathrm{L}}$ and $\tau_{\mathrm{R}} \ll \tau_f = \lambda/(\mu_0 f)$. Such an ABP quickly samples all possible orientations before any translation occurs and the active noise $u_x(t)$ is averaged out from Eq. (3). Thus, self-propulsion is inefficient for the hyper wobbler, which also obeys Eq. (4).

In the opposite regime of a lazy wobbler ($\tau_{\mathrm{R}} \gg \tau_{\mathrm{L}}, \tau_f$), rotational motion is slow. The trajectories $x(t)$ can be thought of as a one-dimensional random walk composed of a sequence of long independent segments $i = 1, 2, \ldots$ with fixed orientations $\boldsymbol{u}_i$ isotropically distributed and randomly changing at random times with rate τ_{R}^{-1}. The active noise term in Eq. (3) is specified by the polar angle $\vartheta \in [0, \pi]$ such that $u_x = \cos\vartheta$; being constant here, the noise term can be absorbed in the shifted driving force $f_{\mathrm{A}}(\vartheta) = f + (v_{\mathrm{A}}/\mu_0)\cos\vartheta$. With this, the dynamic system has the same form as above, $\dot{x} = g(x, f_{\mathrm{A}}(\vartheta))$, and repeating the analysis leading to Eq. (4), one arrives at $v_{\mathrm{D}}(f;\vartheta) = v_{\mathrm{L}} s(f_{\mathrm{A}}(\vartheta)/f_{\mathrm{L}})$. The velocity–force relationship of the lazy wobbler with prescribed orientation ϑ has the same functional form as for the passive particle [Eq. (4)]. Merely the condition $|f_{\mathrm{A}}(\vartheta)| > f_{\mathrm{c}}$ implies a shift of the critical point from $f_{\mathrm{c}} = f_{\mathrm{L}}$ to $f_{\mathrm{L}} - (v_{\mathrm{A}}/\mu_0)\cos\vartheta$. The latter expression depends on ϑ and varies between the maximum and minimum values $f_{\mathrm{c}}^{\pm} = f_{\mathrm{L}} \pm v_{\mathrm{A}}/\mu_0$. In particular, it holds $v_{\mathrm{D}}(f;\vartheta) = 0$ for $f \leqslant f_{\mathrm{c}}^-$ irrespectively of ϑ.

At long times, the random walk implies a uniform average over the orientation, $\langle\cdot\rangle_{\boldsymbol{u}} := (4\pi)^{-1}\int \cdot \sin\vartheta\, \mathrm{d}\vartheta\, \mathrm{d}\varphi$, and we find for the drift velocity $\lim_{t\to\infty}\langle x(t)/t\rangle = \langle v_{\mathrm{D}}(f;\vartheta)\rangle_{\boldsymbol{u}} =: v_{\mathrm{D}}^{(\infty)}(f)$ of the lazy wobbler [64]:

$$v_{\mathrm{D}}^{(\infty)}(f) = \frac{v_{\mathrm{L}}^2}{2v_{\mathrm{A}}}\begin{cases} 0, & f \leqslant f_{\mathrm{c}}^-, \\ w_+(f/f_{\mathrm{L}}), & f_{\mathrm{c}}^- < f < f_{\mathrm{c}}^+, \\ w_+(f/f_{\mathrm{L}}) - w_-(f/f_{\mathrm{L}}), & f \geqslant f_{\mathrm{c}}^+, \end{cases} \tag{6}$$

introducing new scaling functions $w_\pm(y) = w(y \pm v_{\mathrm{A}}/v_{\mathrm{L}})$ with $w(z) = \int_1^z s(y)\mathrm{d}y = [zs(z) - \ln(z + s(z))]/2$. The passive limit [Eq. (4)] is recovered as $v_{\mathrm{A}} \to 0$; in this limit, the two singular points $f_{\mathrm{c}}^{\pm}$ converge to $f_{\mathrm{c}} = f_{\mathrm{L}}$. Due to $w'(z) = s(z)$, the critical exponent β increases by 1, turning the square-root singularity [Eq. (5)] into

$$v_{\mathrm{D}}^{(\infty)}(f \downarrow f_{\mathrm{c}}^-) \sim (f - f_{\mathrm{c}}^-)^{\beta'}, \quad \beta' = 3/2\,. \tag{7}$$

The argument applies similarly for rotational motion in a plane, noting that u_x is distributed differently in this case. Analysis of the leading asymptotic behavior upon $\varepsilon := (f - f_{\mathrm{c}}^-)/f_{\mathrm{L}} \downarrow 0$ yields for $d = 2, 3$ dimensions [64]:

$$v_{\mathrm{D}}^{(\infty)}(\varepsilon \downarrow 0) \simeq \frac{\sqrt{d-1}}{d}\, v_{\mathrm{L}}^{1/2+\beta'} v_{\mathrm{A}}^{1/2-\beta'}\, \varepsilon^{\beta'}\,. \tag{8}$$

The new exponent $\beta' = d/2$ renders the appearance of $v_{\mathrm{D}}^{(\infty)}(f)$ near f_{c}^- smoother than for a passive particle [Fig. 1(b,c)]; yet we stress that Eqs. (6) and (8) predict a sharp transition.

Pictorially, the behavior of $v_{\mathrm{D}}^{(\infty)}(f)$ near $f \approx f_{\mathrm{c}}^-$ may be understood from the random tilts of the potential landscape [Fig. 1(a)]: in an ensemble of particles, only those with orientations pointing sufficiently close towards the direction of the force contribute to the transport: $u_x > u_{x,\mathrm{c}} = 1 - \varepsilon v_{\mathrm{L}}/v_{\mathrm{A}}$ so that $v_{\mathrm{D}}(f;\vartheta) > 0$. Near the transition, $u_{x,\mathrm{c}} \to 1$ and the square-root behavior $v_{\mathrm{D}}(f;\vartheta) \sim (u_x - u_{x,\mathrm{c}})^{1/2}$ is weighted with the distribution of u_x close to 1; the latter is flat for $d = 3$, but divergent $\sim (1-u_x)^{-1/2}$ for $d = 2$. Both factors combine into $\sim (1-u_{x,\mathrm{c}})^{d/2}$ after integration and hence $\beta' = d/2$. Transport near criticality is thus faster for $d = 2$ than for $d = 3$ (Fig. S2 in [64]).

Finite rotational diffusion. For $0 < \tau_{\mathrm{R}} < \infty$, away from the limiting cases, the polar angle $\vartheta(t)$ samples different orientations in the course of time. Regarding the transport, this kind of motion is less efficient than with a fixed orientation in the direction of the driving force ($\vartheta = 0$), whereas the opposite direction ($\vartheta = \pi$) is the most inefficient situation. One concludes that the drift velocity $v_{\mathrm{D}}(f)$ is bounded, $v_{\mathrm{D}}(f;\vartheta=\pi) \leqslant v_{\mathrm{D}}(f) \leqslant v_{\mathrm{D}}(f;\vartheta=0)$; in particular, $v_{\mathrm{D}}(f) = 0$ for $f < f_{\mathrm{c}}^-$ for all values of τ_{R}.

The drift velocity is furthermore bounded by the solutions for the passive particle and the lazy wobbler [Eqs. (4) and (6)]: $v_{\mathrm{D}}^{(\mathrm{p})}(f) \leqslant v_{\mathrm{D}}(f) \leqslant v_{\mathrm{D}}^{(\infty)}(f)$ for all τ_{R} and $f < f_x$ (Fig. 1c) with f_x being the force where the two bounds intersect. For $f > f_x$, the bounds reverse their roles so that for strong driving, counterintuitively, active propulsion slows down transport compared to passive particles.

The described behavior of $v_\mathrm{D}(f)$ is corroborated by precise numerical solutions of the corresponding Fokker–Planck equation, which allowed us to follow $v_\mathrm{D}(f)/v_\mathrm{L}$ down to 10^{-15} [64]. These semi-analytical results suggest a superexponential convergence to the critical point f_c^-,

$$v_\mathrm{D}(f) \simeq v_\mathrm{L} \exp\bigl(-b(f - f_\mathrm{c}^-)^{-\alpha}\bigr)\,, \qquad f \downarrow f_\mathrm{c}^-; \tag{9}$$

the coefficients $\alpha > 1$ and $b > 0$ depend on τ_R and we found that α increases as τ_R is decreased [Fig. 1(d)]. The form of Eq. (9) is in line with predictions from related discrete-time models [67, 68] and it is rooted in a very slow initial increase of the probability that the particle slips along $\boldsymbol{e}_x$ by one wavelength upon increasing $f > f_\mathrm{c}^-$. (For $f < f_\mathrm{c}^-$, this probability is zero.) For $\tau_\mathrm{R} \gg \tau_\mathrm{L}$ and upon increasing f further, the asymptotic behavior of $v_\mathrm{D}(f)$ crosses over to closely follow the lazy-wobbler solution, $v_\mathrm{D}^{(\infty)}(f)$. We conclude that $v_\mathrm{D}(f) > 0$ for $f > f_\mathrm{c}^-$, i.e., the critical point is the same for all $\tau_\mathrm{R} > 0$.

Differential mobility. The differential mobility $\mu(f) = \mathrm{d}v_\mathrm{D}(f)/\mathrm{d}f$ may serve as an alternative measure of the transport which is more sensitive to singular behavior. For finite τ_R, we have calculated $\mu(f)$ from the numerical results for $v_\mathrm{D}(f)$, and $\mu(f)$ is readily obtained for $\tau_\mathrm{R} \to 0$ and $\tau_\mathrm{R} \to \infty$ from Eqs. (4) and (6), respectively [Fig. 1(e)]. In any situation, the potential landscape becomes irrelevant for sufficiently strong driving, $\mu(f \to \infty) = \mu_0$. For the hyper wobbler ($\tau_\mathrm{R} \to 0$), the mobility diverges at the corresponding critical force, $\mu_\mathrm{p}(f \downarrow f_\mathrm{c}) \sim (f - f_\mathrm{c})^{-1/2}$, whereas for the lazy wobbler it vanishes as $\mu_\infty(f \downarrow f_\mathrm{c}^-) \sim (f - f_\mathrm{c}^-)^{1/2}$. In addition, $\mu_\infty(f)$ remains finite but exhibits a cusp at $f = f_\mathrm{c}^+$, pinpointing the presence of a second singular point, at which $\mu_\infty(f)$ is maximal. In between these limiting cases, the mobility exhibits a maximum that, upon increasing τ_R, interpolates in peak height and position between the divergence at $f = f_\mathrm{c}$ ($\tau_\mathrm{R} \ll \tau_\mathrm{L}$) and the cusp at $f = f_\mathrm{c}^+$ ($\tau_\mathrm{R} \gg \tau_\mathrm{L}$). Concomitantly, the left flank of the peak moves from $f = f_\mathrm{c}$ to f_c^-, broadening the peak.

Activity-induced giant diffusion. For passive depinning, the differential mobility was found to be a good proxy of the dispersion coefficient, $D_\mathrm{eff}(f) \propto \mu(f)$, which restores a linear response relation [69]. We have calculated $D_\mathrm{eff}(f)$ for ABPs within the stochastic simulations. For small τ_R, the obtained behavior of $D_\mathrm{eff}(f)$ is strikingly similar to that of $\mu(f)$ [Fig. 1(e,f)]; in particular, $D_\mathrm{eff}(f)/D_\mathrm{free}$ shows a peak near the transition ($f \approx f_\mathrm{c}$), which grows in height without bounds as $\tau_\mathrm{R} \to 0$; here, $D_\mathrm{free} = v_\mathrm{A}^2 \tau_\mathrm{R}/3$ is the effective diffusion of the free ABP. Such giant diffusion was studied for passive particles [70–72] and has been seen in experiments [27, 73]; a similar effect was unveiled recently for circle swimmers subject to gravity [26].

In the lazy-wobbling limit (large τ_R), the corrugated potential induces also an enhanced dispersion. In this regime, the corresponding data for $D_\mathrm{eff}(f)/D_\mathrm{free}$ depend only weakly on τ_R. Invoking again the random walk picture of uncorrelated velocities $v_\mathrm{D}(f;\vartheta_i)$ changing at a "collision rate" τ_R^{-1} yields for the velocity autocorrelation function $Z(t) = \mathrm{Var}[v_\mathrm{D}(f;\vartheta)]_{\boldsymbol{u}} \exp(-t/\tau_\mathrm{R})$ [74]. The Green–Kubo relation gives us $D_\mathrm{eff}(f) = \int_0^\infty Z(t)\mathrm{d}t = \mathrm{Var}[v_\mathrm{D}(f;\vartheta)]_{\boldsymbol{u}}\tau_\mathrm{R}$; the remaining $\boldsymbol{u}$-average is an elementary integral. The lengthy result is given in Eqs. (S21) and (S24) of [64] and drawn in Fig. 1(f) (orange line), which shows that $D_\mathrm{eff}(f)/D_\mathrm{free}$ is maximal near $f \approx (f_\mathrm{c} + f_\mathrm{c}^+)/2$. Expanding $D_\mathrm{max} \approx D_\mathrm{eff}\bigl((f_\mathrm{c} + f_\mathrm{c}^+)/2\bigr)$ for $v_\mathrm{A} \ll v_\mathrm{L}$ yields

$$D_\mathrm{max} \simeq (9 D_\mathrm{free}/8)(v_\mathrm{L}/v_\mathrm{A} + 3/5), \tag{10}$$

which predicts an 6.3-fold enhancement of $D_\mathrm{eff}(f)$ over D_free for $v_\mathrm{A} = 0.2 v_\mathrm{L}$, as is observed in the data for $\tau_\mathrm{R} = 10\tau_\mathrm{L}$ near $f \approx 1.1 f_\mathrm{L}$ [Fig. 1(f)]. We anticipate an arbitrarily large enhancement of the dispersion, $D_\mathrm{max}/D_\mathrm{free} \sim 1/v_\mathrm{A}$, for weakly self-propelled particles with $\tau_\mathrm{R} \gtrsim \tau_\mathrm{L}$.

Conclusions. We have shown that activity impacts the depinning transition as follows: the threshold force is shifted from its value f_c for passive particles to $f_\mathrm{c}^- < f_\mathrm{c}$, which depends on the propulsion strength v_A but not on the persistence time τ_R of rotational motion. A sharp transition is preserved in the presence of active noise, in contrast to the rounding due to translational thermal noise. However, the approach to the transition point from above depends on τ_R and the dimension d of rotational Brownian motion: it obeys different power laws for the limits of the hyper and lazy wobbler with exponents $\beta = 1/2$ (small τ_R) and $\beta' = d/2$ (large τ_R), respectively. In between, $v_\mathrm{D}(f)$ vanishes superexponentially fast, contrasting from the scenario of a τ_R-dependent exponent. For the lazy wobbler, another singular point f_c^+ emerges as the mirror image of f_c^- relative to f_c, where the differential mobility $\mu(f)$ is maximum. Concomitantly, the dispersion coefficient shows a giant enhancement, whose position depends on τ_R. Overall, this qualitative change of the phenomenology is likely beyond the scope of a perturbative treatment of the passive case with τ_R as the small parameter (e.g., [75, 76]). Our work suggests further that probing nonlinear responses [35–37] can contribute to a similar debate for arrested active matter [77–79].

Our predictions appear amenable to experimental tests, e.g., using active colloidal particles driven by external fields (e.g., gravitational [29, 80, 81] or magnetic [25, 33]) over a periodic landscape [48, 58, 60], and potentially for the chemotaxis of bacteria crawling on structured substrates [82, 83]. Experiments on active colloidal monolayers may give insight into the activity-induced depinning of collective variables, and our study is relevant for the melting transition of active colloidal crystals [84].

We also note that the lazy wobbler resembles a run-and-tumble motion with switching rate τ_R^{-1}, which describes the motion of, e.g., *E. coli* bacteria [85, 86].

Finally, the active noise $v_\mathrm{A}\boldsymbol{u}(t)$ differs qualitatively from the thermal, white noise $\boldsymbol{\xi}(t)$, both entering Eq. (1): $v_\mathrm{A}\boldsymbol{u}(t)$ is bounded in magnitude, but $\boldsymbol{\xi}(t)$ can assume arbitrarily large values. Only in the latter case, the probability to surmount the potential barrier is nonzero for any, even small driving force $f \geqslant 0$. Second, the integral $\int_0^t v_\mathrm{A}\boldsymbol{u}(s)\,\mathrm{d}s$ is a finite-variation process, unlike the Wiener process $\int_0^t \boldsymbol{\xi}(s)\,\mathrm{d}s$, and hence yields a drift rather than a diffusion term in the corresponding Fokker–Planck operator (also see [64, 76]). The active noise may thus be interpreted as a random tilting of the potential landscape but not as an intrinsic diffusion. We anticipate that our findings go well beyond the active matter context and apply to any system with a saddle-node bifurcation in the presence of a bounded noise.

We thank Arkady Pikovsky for helpful discussions. Financial support by Deutsche Forschungsgemeinschaft (DFG, German Research Foundation) under Germany's Excellence Strategy—MATH+: The Berlin Mathematics Research Center (EXC-2046/1)—Project No. 390685689 (Subprojects AA1-18 and EF4-10) and further under Project No. 523950429 is gratefully acknowledged.

* straube@zib.de

[1] D. S. Fisher, Collective transport in random media: from superconductors to earthquakes, Phys. Rep. **301**, 113 (1998).
[2] S. Brazovskii and T. Nattermann, Pinning and sliding of driven elastic systems: from domain walls to charge density waves, Adv. Phys. **53**, 177 (2004).
[3] C. Reichhardt and C. J. O. Reichhardt, Depinning and nonequilibrium dynamic phases of particle assemblies driven over random and ordered substrates: a review, Rep. Prog. Phys. **80**, 026501 (2017).
[4] F. Haudin, R. G. Elías, R. G. Rojas, U. Bortolozzo, M. G. Clerc, and S. Residori, Driven front propagation in 1d spatially periodic media, Phys. Rev. Lett. **103**, 128003 (2009).
[5] A. Carpio and L. L. Bonilla, Wave front depinning transition in discrete one-dimensional reaction-diffusion systems, Phys. Rev. Lett. **86**, 6034 (2001).
[6] F. Martinez-Pedrero, P. Tierno, T. H. Johansen, and A. V. Straube, Regulating wave front dynamics from the strongly discrete to the continuum limit in magnetically driven colloidal systems, Sci. Rep. **6**, 19932 (2016).
[7] Y. Jiang, Y. Sun, J. W. Drelich, and C.-H. Choi, Topography-dependent effective contact line in droplet depinning, Phys. Rev. Lett. **125**, 184502 (2020).
[8] K. J. A. Franke, B. Van de Wiele, Y. Shirahata, S. J. Hämäläinen, T. Taniyama, and S. van Dijken, Reversible electric-field-driven magnetic domain-wall motion, Phys. Rev. X **5**, 011010 (2015).
[9] S. Woo, T. Delaney, and G. S. D. Beach, Magnetic domain wall depinning assisted by spin wave bursts, Nat. Phys. **13**, 448 (2017).
[10] N. Bauer, S. M. Neumayer, P. Maksymovych, and M. O. Lavrentovich, Structures and velocities of noisy ferroelectric domain walls, Phys. Rev. Materials **6**, 124401 (2022).
[11] G. Blatter, M. V. Feigel'man, V. B. Geshkenbein, A. I. Larkin, and V. M. Vinokur, Vortices in high-temperature superconductors, Rev. Mod. Phys. **66**, 1125 (1994).
[12] M. Buchacek, R. Willa, V. B. Geshkenbein, and G. Blatter, Strong pinning theory of thermal vortex creep in type-II superconductors, Phys. Rev. B **100**, 014501 (2019).
[13] Y. Fily, E. Olive, N. Di Scala, and J. C. Soret, Critical behavior of plastic depinning of vortex lattices in two dimensions: Molecular dynamics simulations, Phys. Rev. B **82**, 134519 (2010).
[14] S.-Z. Lin, C. Reichhardt, C. D. Batista, and A. Saxena, Particle model for skyrmions in metallic chiral magnets: Dynamics, pinning, and creep, Phys. Rev. B **87**, 214419 (2013).
[15] A. Vanossi, N. Manini, M. Urbakh, S. Zapperi, and E. Tosatti, *Colloquium*: Modeling friction: From nanoscale to mesoscale, Rev. Mod. Phys. **85**, 529 (2013).
[16] A. Bylinskii, D. Gangloff, and V. Vuletić, Tuning friction atom-by-atom in an ion-crystal simulator, Science **348**, 1115 (2015).
[17] A. Vanossi, C. Bechinger, and M. Urbakh, Structural lubricity in soft and hard matter systems, Nat. Commun. **11**, 4657 (2020).
[18] T. Brazda, A. Silva, N. Manini, A. Vanossi, R. Guerra, E. Tosatti, and C. Bechinger, Experimental observation of the Aubry transition in two-dimensional colloidal monolayers, Phys. Rev. X **8**, 011050 (2018).
[19] O. Hod, E. Meyer, Q. Zheng, and M. Urbakh, Structural superlubricity and ultralow friction across the length scales, Nature **563**, 485 (2018).
[20] M. P. N. Juniper, A. V. Straube, R. Besseling, D. G. A. L. Aarts, and R. P. A. Dullens, Microscopic dynamics of synchronization in driven colloids, Nat. Commun. **6**, 7187 (2015).
[21] P. T. Korda, M. B. Taylor, and D. G. Grier, Kinetically locked-in colloidal transport in an array of optical tweezers, Phys. Rev. Lett. **89**, 128301 (2002).
[22] M. Balvin, E. Sohn, T. Iracki, G. Drazer, and J. Frechette, Directional locking and the role of irreversible interactions in deterministic hydrodynamics separations in microfluidic devices, Phys. Rev. Lett. **103**, 078301 (2009).
[23] M. P. N. Juniper, U. Zimmermann, A. V. Straube, R. Besseling, D. G. A. L. Aarts, H. Löwen, and R. P. A. Dullens, Dynamic mode locking in a driven colloidal system: experiments and theory, New J. Phys. **19**, 013010 (2017).
[24] X. Cao, E. Panizon, A. Vanossi, N. Manini, and C. Bechinger, Orientational and directional locking of colloidal clusters driven across periodic surfaces, Nat. Phys. **15**, 776 (2019).
[25] R. L. Stoop, A. V. Straube, T. H. Johansen, and P. Tierno, Collective directional locking of colloidal monolayers on a periodic substrate, Phys. Rev. Lett. **124**, 058002 (2020).
[26] O. Chepizhko and T. Franosch, Resonant diffusion of a gravitactic circle swimmer, Phys. Rev. Lett. **129**, 228003 (2022).
[27] M. Evstigneev, O. Zvyagolskaya, S. Bleil, R. Eichhorn,

C. Bechinger, and P. Reimann, Diffusion of colloidal particles in a tilted periodic potential: Theory versus experiment, Phys. Rev. E **77**, 041107 (2008).

[28] A. V. Straube and P. Tierno, Synchronous vs. asynchronous transport of a paramagnetic particle in a modulated ratchet potential, EPL (Europhys. Lett.) **103**, 28001 (2013).

[29] X.-g. Ma, P.-Y. Lai, B. J. Ackerson, and P. Tong, Colloidal transport and diffusion over a tilted periodic potential: dynamics of individual particles, Soft Matter **11**, 1182 (2015).

[30] M. P. N. Juniper, A. V. Straube, D. G. A. L. Aarts, and R. P. A. Dullens, Colloidal particles driven across periodic optical-potential-energy landscapes, Phys. Rev. E **93**, 012608 (2016).

[31] A. Pertsinidis and X. S. Ling, Statics and dynamics of 2d colloidal crystals in a random pinning potential, Phys. Rev. Lett. **100**, 028303 (2008).

[32] T. Bohlein, J. Mikhael, and C. Bechinger, Observation of kinks and antikinks in colloidal monolayers driven across ordered surfaces, Nat. Mater. **11**, 126 (2011).

[33] P. Tierno, Depinning and collective dynamics of magnetically driven colloidal monolayers, Phys. Rev. Lett. **109**, 198304 (2012).

[34] M. Hülsberg and S. H. L. Klapp, Depinning dynamics of confined colloidal dispersions under oscillatory shear, Phys. Rev. E **107**, 014603 (2023).

[35] D. Winter and J. Horbach, Nonlinear active microrheology in a glass-forming soft-sphere mixture, J. Chem. Phys. **138**, 12A512 (2013).

[36] N. Şenbil, M. Gruber, C. Zhang, M. Fuchs, and F. Scheffold, Observation of strongly heterogeneous dynamics at the depinning transition in a colloidal glass, Phys. Rev. Lett. **122**, 108002 (2019).

[37] M. Gruber, A. M. Puertas, and M. Fuchs, Critical force in active microrheology, Phys. Rev. E **101**, 012612 (2020).

[38] P. Romanczuk, M. Bär, W. Ebeling, B. Lindner, and L. Schimansky-Geier, Active Brownian particles, Eur. Phys. J. Special Topics **202**, 1 (2012).

[39] I. S. Aranson, Active colloids, Physics-Uspekhi **56**, 79 (2013).

[40] J. Elgeti, R. G. Winkler, and G. Gompper, Physics of microswimmers—single particle motion and collective behavior: a review, Rep. Prog. Phys. **78**, 056601 (2015).

[41] C. Bechinger, R. Di Leonardo, H. Löwen, C. Reichhardt, G. Volpe, and G. Volpe, Active particles in complex and crowded environments, Rev. Mod. Phys. **88**, 045006 (2016).

[42] A. Zöttl and H. Stark, Emergent behavior in active colloids, J. Phys.: Condens. Matter **28**, 253001 (2016).

[43] B. J. Nelson, I. K. Kaliakatsos, and J. J. Abbott, Microrobots for minimally invasive medicine, Annu. Rev. Biomed. Eng. **12**, 55 (2010).

[44] S. Palagi and P. Fischer, Bioinspired microrobots, Nat. Rev. Mater. **3**, 113 (2018).

[45] Y. Alapan, O. Yasa, O. Schauer, J. Giltinan, A. F. Tabak, V. Sourjik, and M. Sitti, Soft erythrocyte-based bacterial microswimmers for cargo delivery, Sci. Robot. **3**, eaar4423 (2018).

[46] Z. Xiao, M. Wei, and W. Wang, A review of micromotors in confinements: Pores, channels, grooves, steps, interfaces, chains, and swimming in the bulk, ACS Appl. Mater. Interfaces **11**, 6667 (2019).

[47] M. Reza Shaebani, A. Wysocki, R. G. Winkler, G. Gompper, and H. Rieger, Computational models for active matter, Nat. Rev. Phys. **2**, 181 (2020).

[48] U. Choudhury, A. V. Straube, P. Fischer, J. G. Gibbs, and F. Höfling, Active colloidal propulsion over a crystalline surface, New J. Phys. **19**, 125010 (2017).

[49] A. V. Straube, J. M. Pagès, P. Tierno, J. Ignés-Mullol, and F. Sagués, Collective dynamics and conformal ordering in electrophoretically driven nematic colloids, Phys. Rev. Research **1**, 022008 (2019).

[50] A. Ryabov and M. Tasinkevych, Mechanochemical active ratchet, Sci. Rep. **13**, 20572 (2023).

[51] P. Bag, S. Nayak, T. Debnath, and P. K. Ghosh, Directed autonomous motion and chiral separation of self-propelled Janus particles in convection roll arrays, J. Phys. Chem. Lett. **13**, 11413 (2022).

[52] P. K. Ghosh, P. Hänggi, F. Marchesoni, and F. Nori, Giant negative mobility of Janus particles in a corrugated channel, Phys. Rev. E **89**, 062115 (2014).

[53] P. Rizkallah, A. Sarracino, O. Bénichou, and P. Illien, Absolute negative mobility of an active tracer in a crowded environment, Phys. Rev. Lett. **130**, 218201 (2023).

[54] S. Pattanayak, R. Das, M. Kumar, and S. Mishra, Enhanced dynamics of active Brownian particles in periodic obstacle arrays and corrugated channels, Eur. Phys. J. E **42**, 62 (2019).

[55] S. Leitmann, F. Höfling, and T. Franosch, Tube concept for entangled stiff fibers predicts their dynamics in space and time, Phys. Rev. Lett. **117**, 097801 (2016); Dynamically crowded solutions of infinitely thin Brownian needles, Phys. Rev. E **96**, 012118 (2017).

[56] F. Höfling and A. V. Straube, Langevin equations and a geometric integration scheme for the overdamped limit of homogeneous rotational Brownian motion (2024), arXiv:2403.04501 [cond-mat.stat-mech].

[57] M. Enculescu and H. Stark, Active colloidal suspensions exhibit polar order under gravity, Phys. Rev. Lett. **107**, 058301 (2011).

[58] J. G. Gibbs, Shape- and material-dependent self-propulsion of photocatalytic active colloids, interfacial effects, and dynamic interparticle interactions, Langmuir **36**, 6938 (2019).

[59] V. Carrasco-Fadanelli and I. Buttinoni, Sedimentation and levitation of catalytic active colloids, Phys. Rev. Research **5**, L012018 (2023).

[60] Y. Wen, Z. Li, H. Wang, J. Zheng, J. Tang, P.-Y. Lai, X. Xu, and P. Tong, Activity-assisted barrier crossing of self-propelled colloids over parallel microgrooves, Phys. Rev. E **107**, L032601 (2023).

[61] R. L. Stratonovich, *Topics in the Theory of Random Noise*, Vol. II (Gordon and Breach, New York, 1967).

[62] A. A. Middleton, Thermal rounding of the charge-density-wave depinning transition, Phys. Rev. B **45**, 9465 (1992).

[63] A. B. Kolton and E. A. Jagla, Thermally rounded depinning of an elastic interface on a washboard potential, Phys. Rev. E **102**, 052120 (2020).

[64] See Supplemental Material at [URL] for a description of the numerics and for intermediate steps of the mathematical derivations.

[65] S. H. Strogatz, *Nonlinear Dynamics And Chaos: With Applications To Physics, Biology, Chemistry, And Engineering* (Addison-Wesley, Reading, Massachusetts, 1994).

[66] For fast active motion, $v_A \geqslant v_L$, the particle depins for any $f > 0$; we exclude this trivial situation here.
[67] G. Olicón Méndez, *Critical behaviour of random diffeomorphisms: quasi-stationary measures and escape times*, Ph.D. thesis, Imperial College London (2020).
[68] V. Chigarev, A. Kazakov, and A. Pikovsky, Attractor–repeller collision and the heterodimensional dynamics, Chaos **33**, 063113 (2023).
[69] G. Costantini and F. Marchesoni, Threshold diffusion in a tilted washboard potential, EPL (Europhys. Lett.) **48**, 491 (1999).
[70] P. Reimann, C. Van den Broeck, H. Linke, P. Hänggi, J. M. Rubi, and A. Pérez-Madrid, Giant acceleration of free diffusion by use of tilted periodic potentials, Phys. Rev. Lett. **87**, 010602 (2001); Diffusion in tilted periodic potentials: Enhancement, universality, and scaling, Phys. Rev. E **65**, 031104 (2002).
[71] N. J. López-Alamilla, M. W. Jack, and K. J. Challis, Enhanced diffusion and the eigenvalue band structure of Brownian motion in tilted periodic potentials, Phys. Rev. E **102**, 042405 (2020).
[72] B. Lindner and I. M. Sokolov, Giant diffusion of underdamped particles in a biased periodic potential, Phys. Rev. E **93**, 042106 (2016).
[73] R. L. Stoop, A. V. Straube, and P. Tierno, Enhancing nanoparticle diffusion on a unidirectional domain wall magnetic ratchet, Nano Lett. **19**, 433 (2018).
[74] P. Ehrenfest and T. Ehrenfest, *The Conceptual Foundations of the Statistical Approach in Mechanics* (Cornell University Press, Ithaca, 1959).
[75] É. Fodor, C. Nardini, M. E. Cates, J. Tailleur, P. Visco, and F. van Wijland, How far from equilibrium is active matter?, Phys. Rev. Lett. **117**, 038103 (2016).
[76] G. Szamel, Self-propelled particle in an external potential: Existence of an effective temperature, Phys. Rev. E **90**, 012111 (2014).
[77] K. Paul, A. Mutneja, S. K. Nandi, and S. Karmakar, Dynamical heterogeneity in active glasses is inherently different from its equilibrium behavior, Proc. Natl. Acad. Sci. **120**, e2217073120 (2023).
[78] V. E. Debets and L. M. C. Janssen, Active glassy dynamics is unaffected by the microscopic details of self-propulsion, J. Chem. Phys. **157**, 224902 (2022); L. M. C. Janssen, Active glasses, J. Phys.: Condens. Matter **31**, 503002 (2019).
[79] N. Klongvessa, F. Ginot, C. Ybert, C. Cottin-Bizonne, and M. Leocmach, Active glass: Ergodicity breaking dramatically affects response to self-propulsion, Phys. Rev. Lett. **123**, 248004 (2019).
[80] J. Palacci, C. Cottin-Bizonne, C. Ybert, and L. Bocquet, Sedimentation and effective temperature of active colloidal suspensions, Phys. Rev. Lett. **105**, 088304 (2010).
[81] A. L. Thorneywork, J. L. Abbott, D. G. A. L. Aarts, and R. P. A. Dullens, Two-dimensional melting of colloidal hard spheres, Phys. Rev. Lett. **118**, 158001 (2017).
[82] G. Amselem, M. Theves, A. Bae, E. Bodenschatz, and C. Beta, A stochastic description of Dictyostelium chemotaxis, PLoS ONE **7**, e37213 (2012).
[83] L. Rußbach, M. Ecke, J. O. Rädler, C. Leu, and G. Gerisch, Cells responding to chemoattractant on a structured substrate, Biophys. J. **121**, 2557 (2022).
[84] H. Massana-Cid, C. Maggi, N. Gnan, G. Frangipane, and R. Di Leonardo, Multiple temperatures and melting of a colloidal active crystal (2024), arXiv:2401.09911 [cond-mat.soft].
[85] M. J. Schnitzer, Theory of continuum random walks and application to chemotaxis, Phys. Rev. E **48**, 2553 (1993).
[86] A. P. Solon, M. E. Cates, and J. Tailleur, Active Brownian particles and run-and-tumble particles: A comparative study, Eur. Phys. J. Special Topics **224**, 1231 (2015).
[87] P. Reimann, Brownian motors: noisy transport far from equilibrium, Phys. Rep. **361**, 57 (2002).

SUPPLEMENTAL MATERIAL

NUMERICS OF THE ACTIVE BROWNIAN PARTICLE (ABP) MODEL

Stochastic simulation of the Itō–Langevin equations

For the stochastic simulation of the ABP model given by Eqs. (2) and (3) in the main text, we have generated, for each force f, up to 5×10^5 random trajectories $x(t)$ of length $5\times10^4\tau_\mathrm{L}$. To this end, we combined the Euler(–Maruyama) integration for the translational motion and a geometric integration scheme [56] for the rotational Brownian motion, using an integration time step of $\Delta t = 10^{-3}\tau_\mathrm{L}$. In addition, we have applied a simple antithetic variance reduction technique, where for every noise realization $\boldsymbol{\omega}(t)$ one obtains two trajectories: one with $\boldsymbol{\omega}(t)$ and one with $-\boldsymbol{\omega}(t)$, exploiting the inflection symmetry of the noise.

Numerical solution of the Fokker–Planck equation

The Fokker–Planck equation (FPE) corresponding to the Itō–Langevin Eqs. (1) and (2) of the main text reads

$$\partial_t p(\boldsymbol{r},\boldsymbol{u},t) = -\nabla\cdot\left[\mu_0(\boldsymbol{f}-\nabla U(\boldsymbol{r})) + v_\mathrm{A}\boldsymbol{u}\right] p(\boldsymbol{r},\boldsymbol{u},t) + \tau_\mathrm{R}^{-1} L_{\boldsymbol{u}}\, p(\boldsymbol{r},\boldsymbol{u},t)\,, \tag{S1}$$

where $p(x,\boldsymbol{u},t)$ is the joint probability density of the position x and the orientation $\boldsymbol{u}$ at time t and $L_{\boldsymbol{u}}$ denotes the Laplace–Beltrami operator on the d-dimensional unit sphere. For the one-dimensional corrugated potential landscape discussed in this work, only the projection $x=\boldsymbol{r}\cdot\boldsymbol{e}_x$ and the polar angle ϑ such that $z:=\cos(\vartheta)=\boldsymbol{u}\cdot\boldsymbol{e}_x$ are relevant. Then, Eq. (S1) reduces to

$$\partial_t p(x,z,t) = -\partial_x\left[\mu_0 f - v_\mathrm{L}\sin(kx) + v_\mathrm{A} z\right] p(x,z,t) + \tau_\mathrm{R}^{-1}\partial_z\big(1-z^2\big)\partial_z\, p(x,z,t)\,, \tag{S2}$$

which is the FPE corresponding to Eqs. (2) and (3) of the main text. The domain of $p(x,z,t)$ is $x\in\mathbb{R}$, $z\in[-1,1]$, and $t\geqslant 0$.

Exploiting the inherent x-periodicity of the problem, we proceed to the reduced probability density [87] $\hat p(x,z,t) := \sum_{n=-\infty}^{\infty} p(x+n\lambda,z,t)$, which satisfies Eq. (S2) for $x\in[0,\lambda]$ with periodic boundary conditions, $\hat p(x,z,t)=\hat p(x+\lambda,z,t)$ with $\lambda=2\pi/k$. We recall further that the eigenfunctions of the $d=3$ rotational diffusion operator are the Legendre polynomials $P_\ell(z)$, i.e.,

$$\partial_z\big(1-z^2\big)\partial_z P_\ell(z) = -\ell(\ell+1)P_\ell(z)\,; \qquad \ell\in\mathbb{N}_0\,. \tag{S3}$$

The periodicity of $\hat p(x,z,t)$ in x together with Eq. (S3) suggest to represent the solution as a Fourier–Legendre series,

$$\hat p(x,z,t) = \sum_{n\in\mathbb{Z}}\sum_{\ell\geqslant 0} c_{n\ell}(t)\mathrm{e}^{\mathrm{i}nkx}P_\ell(z)\,. \tag{S4}$$

The time evolution of the coefficients $c_{n\ell}(t)$ is implied by Eq. (S2) and one finds:

$$\dot c_{n0} = -\,\mathrm{i}nk\left[\mu_0 f c_{n0} - \frac{v_\mathrm{L}}{2\mathrm{i}}(c_{n-1,0}-c_{n+1,0})\right] - \mathrm{i}nkv_\mathrm{A}\frac{c_{n1}}{3}\,; \qquad \ell=0, \tag{S5a}$$

$$\begin{aligned}\dot c_{n\ell} = &-\,\mathrm{i}nk\left[\mu_0 f c_{n\ell} - \frac{v_\mathrm{L}}{2\mathrm{i}}(c_{n-1,\ell}-c_{n+1,\ell})\right]\\ &-\,\mathrm{i}nkv_\mathrm{A}\left(\frac{\ell}{2\ell-1}c_{n,\ell-1} + \frac{\ell+1}{2\ell+3}c_{n,\ell+1}\right) - \tau_\mathrm{R}^{-1}\ell(\ell+1)c_{n\ell}\,; \qquad \ell>0.\end{aligned} \tag{S5b}$$

For the stationary solution, the left hand sides are set to zero, $\dot c_{n\ell}=0$, and Eq. (S5) becomes a linear system in the coefficients $c_{n\ell}$. The normalization condition $\int \hat p(x,z,t)\,\mathrm{d}x\mathrm{d}z=1$ implies $c_{00}=1/2$, which renders the linear system inhomogeneous. We truncated the series (S4) symmetrically to keep only terms with $-N\leqslant n\leqslant N$ and $0\leqslant \ell\leqslant L$ and solved the system of $(2N+1)\times(L+1)$ equations numerically using standard BLAS routines.

The mean speed $v_\mathrm{D}(f) = \lim_{t\to\infty}\langle\dot x(t)\rangle$ is the integral of the x-component of the probability flux $\langle\dot x(t)\rangle = \int \hat\jmath_x(x,z,t)\,\mathrm{d}x\mathrm{d}z$ with $\hat\jmath_x(x,z,t) = (\mu_0 f - v_\mathrm{L}\sin(kx) + v_\mathrm{A}z)\hat p(x,z,t)$ and, upon using Eq. (S4), it is calculated from the expansion coefficients as

$$v_\mathrm{D}(f) = \mu_0 f + 2v_\mathrm{L}\,\mathrm{Im}\,c_{1,0} + \frac{2}{3}v_\mathrm{A}c_{0,1}\,. \tag{S6}$$

The numerical results shown in Fig. S1 and in Fig. 1(c) of the main text were obtained for $N=10\,000$ and $L=30$. The different orders of magnitude for N and L were chosen to account for the observation that the eigenvalues of ∇ scale as n, whereas the eigenvalues of $L_{\boldsymbol{u}}$ scale as $\ell(\ell+1)$.

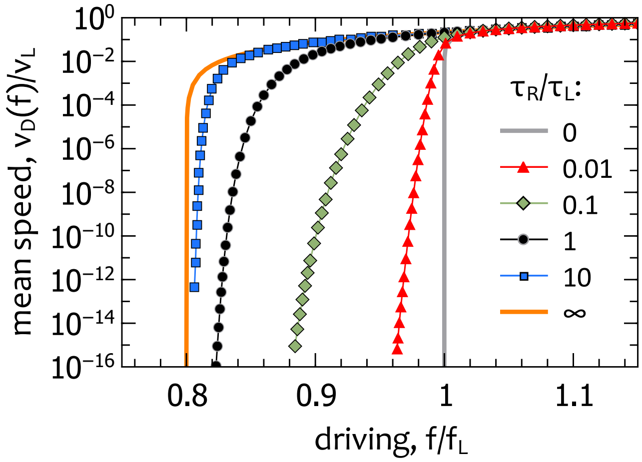

FIG. S1. Drift velocity $v_\mathrm{D}(f)$ as function of the driving force f was obtained from the numerical FPE solution [Eq. (S6)] with the self-propulsion velocity fixed to $v_\mathrm{A} = 0.2v_\mathrm{L}$. The same data are shown in Fig. 1c of the main text on a super-logarithmic scale.

DRIFT VELOCITY AND DISPERSION COEFFICIENT OF LAZY WOBBLERS

Random walk model

As described in the main text, the trajectories $x(t)$ in the regime of the lazy wobbler ($\tau_\mathrm{R} \gg \tau_\mathrm{L}$ and $\tau_R \gg \tau_f$) are approximated by a one-dimensional random walk (or "flight") such that the orientation of the particle changes instantaneously at random times with a rate τ_R^{-1}. In this heuristic model, the orientation $\boldsymbol{u}(t)$ consists of piecewise constant segments $\boldsymbol{u}_i$ of random durations τ_i for $i = 1, 2, \dots$. For the depinning problem, we may equivalently use the angles ϑ_i such that $\cos\vartheta_i = \boldsymbol{u}_i \cdot \boldsymbol{e}_x$. Given a fixed orientation $\boldsymbol{u}_i$ (or ϑ_i), the particle moves at the velocity $v_\mathrm{D}(f;\vartheta_i)$ for a time span τ_i. Then, assuming $x(0) = 0$, the spatial displacement after time t is

$$x(t) = \sum_{i=1}^{N(t)} v_\mathrm{D}(f;\vartheta_i)\tau_i\,, \tag{S7}$$

where $N(t)$ is counting the reorientation events up to and including time $t = \sum_{i=1}^{N(t)} \tau_i$. The resulting trajectories $x(t)$ correspond exactly to the motion of run-and-tumble particles.

Following the ideas of Boltzmann's Stoßzahlansatz (molecular chaos hypothesis) [74], the reorientation events ("collisions") are assumed to be independent and combine exponentially distributed times τ_i between subsequent collisions with orientations $\boldsymbol{u}_i$ that are sampled independently from the equilibrium distribution, i.e., a uniform distribution on the unit sphere, $|\boldsymbol{u}| = 1$. As a consequence, $N(t)$ is a Poisson process with parameter τ_R^{-1}.

Drift velocity

For the drift velocity (or: mean speed), one finds from Eq. (S7):

$$\begin{aligned} v_\mathrm{D}^{(\infty)}(f) &= \lim_{t\to\infty} \frac{x(t)}{t} \\ &= \lim_{N\to\infty} \frac{1}{N}\sum_{i=1}^{N} v_\mathrm{D}(f;\vartheta_i)\tau_i \Big/ \frac{1}{N}\sum_{i=1}^{N}\tau_i \\ &= \frac{\langle v_\mathrm{D}(f;\vartheta_i)\rangle_{\boldsymbol{u}}\langle\tau_i\rangle}{\langle\tau_i\rangle} \\ &= \frac{1}{4\pi}\int v_\mathrm{D}(f;\vartheta)\sin(\vartheta)\,\mathrm{d}\vartheta\mathrm{d}\varphi\,. \end{aligned} \tag{S8}$$

In the second line, we have used that $N(t \to \infty) \to \infty$ monotonically, which permits that the limit $t \to \infty$ is replaced by letting $N \to \infty$. The third line follows from the strong law of large numbers and the independence of ϑ_i and τ_i. The last line of Eq. (S8) represents the orientation-averaged drift velocity, $\langle v_\mathrm{D}(f;\vartheta_i)\rangle_{\boldsymbol{u}}$. We rewrite the integrand, as in the main text, in terms of $v_\mathrm{D}(f;\vartheta) = v_\mathrm{L} s(f_\mathrm{A}(\vartheta)/f_\mathrm{L})$ with the effective driving force $f_\mathrm{A}(\vartheta) = f + (v_\mathrm{A}/\mu_0)\cos\vartheta$ and $s(y) = \sqrt{y^2-1}$ for $|y| > 1$ and $s(y) = 0$ otherwise. Substituting $u_x = \cos\vartheta$, the $\boldsymbol{u}$-average is calculated as:

$$\begin{aligned} v_\mathrm{D}^{(\infty)}(f) &= \frac{v_\mathrm{L}}{2}\int_{-1}^{1} s\big(f/f_\mathrm{L} + (v_\mathrm{A}/v_\mathrm{L})u_x\big)\,\mathrm{d}u_x \\ &= \frac{v_\mathrm{L}^2}{2v_\mathrm{A}} \int\limits_{\max(y_-,1)}^{\max(y_+,1)} s(y)\,\mathrm{d}y\,, \end{aligned} \tag{S9}$$

after substituting $y = f_\mathrm{A}(\vartheta)/f_\mathrm{L} = f/f_\mathrm{L} + (v_\mathrm{A}/v_\mathrm{L})u_x$ for u_x. The integral bounds $y_\pm = f/f_\mathrm{L} \pm v_\mathrm{A}/v_\mathrm{L}$ have been tightened to the condition $|y| > 1$, where the integrand is nonzero. The remaining integral is elementary:

$$w(y) := \int_1^y s(y')\mathrm{d}y' = \frac{1}{2}\left[ys(y) - \ln\big(y + s(y)\big)\right]. \tag{S10}$$

Introducing $w_\pm(f/f_\mathrm{L}) := w(y_\pm) = w(y \pm v_\mathrm{A}/v_\mathrm{L})$ and noting that $w_-(f_\mathrm{c}^+/f_\mathrm{L}) = w(1) = 0$, we obtain the result quoted in Eq. (6) of the main text:

$$v_\mathrm{D}^{(\infty)}(f) = \frac{v_\mathrm{L}^2}{2v_\mathrm{A}}\begin{cases} 0, & f \leqslant f_\mathrm{c}^-\,, \\ w_+(f/f_\mathrm{L}), & f_\mathrm{c}^- < f < f_\mathrm{c}^+\,, \\ w_+(f/f_\mathrm{L}) - w_-(f/f_\mathrm{L}), & f \geqslant f_\mathrm{c}^+\,. \end{cases} \tag{S11}$$

Critical behavior

To obtain the critical behavior of the drift velocity, we introduce the distance to the critical point, $\varepsilon = (f - f_\mathrm{c}^-)/f_\mathrm{L}$, and find the leading term in an asymptotic expansion of the integral in Eq. (S9). Restricting to $0 < \varepsilon < 2v_\mathrm{A}/v_\mathrm{L}$, it holds $y_+ = 1 + \varepsilon$ and $y_- = 1 + \varepsilon - 2v_\mathrm{A}/v_\mathrm{L} < 1$, which simplifies the integral bounds. Introducing a new integration variable $0 \leqslant \eta \leqslant 1$ such that $y = 1 + \eta\varepsilon$ yields:

$$\begin{aligned} v_\mathrm{D}^{(\infty)}(f = f_\mathrm{c}^- + \varepsilon f_\mathrm{L}) &= \frac{v_\mathrm{L}^2}{2v_\mathrm{A}}\int\limits_1^{1+\varepsilon} s(y)\,\mathrm{d}y = \frac{v_\mathrm{L}^2}{2v_\mathrm{A}}\,\varepsilon\int\limits_0^1 \sqrt{2\eta\varepsilon}\,[1 + O(\varepsilon)]\,\mathrm{d}\eta \\ &= \frac{v_\mathrm{L}^2}{2v_\mathrm{A}}\frac{2\sqrt{2}}{3}\,\varepsilon^{3/2}\,[1 + O(\varepsilon)]\,. \end{aligned} \tag{S12}$$

We used that $s(y)$ is bounded on the domain of integration, which permits interchanging the η-integral with the expansion for $\varepsilon \to 0$. Hence,

$$v_\mathrm{D}^{(\infty)}(f \downarrow f_\mathrm{c}^-) \simeq \frac{\sqrt{2}}{3}\frac{v_\mathrm{L}^2}{v_\mathrm{A}}\,\varepsilon^{3/2} \sim (f - f_\mathrm{c}^-)^{3/2}\,. \tag{S13}$$

Alternatively, the same result is obtained by expanding $w_+(1+\varepsilon)$ defined after Eq. (S10).

Extension to rotational motion in the plane

The preceding analysis of the lazy-wobbling limit has a straightforward extension to ABP models with two-dimensional rotational motion, where the self-propulsion velocity is constrained to the plane of translational motion. The essential difference is that the orientation vector $\boldsymbol{u}$ is uniformly distributed on a circle rather than on a sphere, which has implications for the integrals implementing the $\boldsymbol{u}$-average. For the mean speed, Eq. (S8) is replaced by

$$v_\mathrm{D}^{(\infty)}(f) = \frac{1}{\pi}\int_0^\pi v_\mathrm{D}(f;\vartheta)\,\mathrm{d}\vartheta\,, \tag{S14}$$

where we stick to a representation in terms of the polar angle $\vartheta \in [0, \pi]$. Relative to Eq. (S8), the factor $\sin(\vartheta)$ is missing from the differential of the solid angle. Nevertheless, we substitute $u_x = \cos(\vartheta)$ with $\mathrm{d}u_x = \sin(\vartheta)\,\mathrm{d}\vartheta = \sqrt{1-u_x^2}\,\mathrm{d}\vartheta$ and, subsequently, introduce y as above. With this, the expression corresponding to Eq. (S9) reads

$$\begin{aligned} v_{\mathrm{D}}^{(\infty)}(f) &= \frac{v_{\mathrm{L}}}{\pi} \int_{-1}^{1} \frac{s\big(f/f_{\mathrm{L}} + (v_{\mathrm{A}}/v_{\mathrm{L}})u_x\big)}{\sqrt{1-u_x^2}}\,\mathrm{d}u_x \\ &= \frac{v_{\mathrm{L}}^2}{\pi v_{\mathrm{A}}} \int\limits_{\max(y_-,1)}^{\max(y_+,1)} \frac{s(y)}{\sqrt{1-r(y)^2}}\,\mathrm{d}y\,, \end{aligned} \tag{S15}$$

upon replacing $u_x = r(y) := (v_{\mathrm{L}}/v_{\mathrm{A}})(y - f/f_{\mathrm{L}})$ by y and $y_\pm = f/f_{\mathrm{L}} \pm v_{\mathrm{A}}/v_{\mathrm{L}}$, as before.

In the absence of an explicit form for the integral in Eq. (S15), we determine the critical behavior close to the critical point analogously as above for $d = 3$. Writing again $f = f_{\mathrm{c}}^- + \varepsilon f_{\mathrm{L}}$, it holds $r(y;\varepsilon) = 1 + (v_{\mathrm{L}}/v_{\mathrm{A}})(y - 1 - \varepsilon)$. For $0 < \varepsilon < 2v_{\mathrm{A}}/v_{\mathrm{L}}$, we thus have

$$v_{\mathrm{D}}^{(\infty)}(f = f_{\mathrm{c}}^- + \varepsilon f_{\mathrm{L}}) = \frac{v_{\mathrm{L}}^2}{\pi v_{\mathrm{A}}} \int\limits_{1}^{1+\varepsilon} \frac{s(y)}{\sqrt{1-r(y;\varepsilon)^2}}\,\mathrm{d}y\,. \tag{S16}$$

Passing on to the integration variable η such that $y = 1 + \eta\varepsilon$, the leading order in ε is obtained by letting $\varepsilon \to 0$ in the integrand:

$$\begin{aligned} v_{\mathrm{D}}^{(\infty)}(f = f_{\mathrm{c}}^- + \varepsilon f_{\mathrm{L}}) &= \frac{v_{\mathrm{L}}^2}{\pi v_{\mathrm{A}}} \int_0^1 \frac{\sqrt{2\eta\varepsilon + O(\varepsilon^2)}}{\sqrt{2(v_{\mathrm{L}}/v_{\mathrm{A}})(1-\eta)\varepsilon + O(\varepsilon^2)}}\,\varepsilon \mathrm{d}\eta \\ &\simeq \frac{v_{\mathrm{L}}^{3/2}\varepsilon}{\pi v_{\mathrm{A}}^{1/2}} \int_0^1 \sqrt{\eta/(1-\eta)}\,\mathrm{d}\eta \\ &= \frac{v_{\mathrm{L}}^{3/2}\varepsilon}{2v_{\mathrm{A}}^{1/2}}\,; \end{aligned} \tag{S17}$$

the integral in the last step evaluates to $\pi/2$. Thus close to the critical point, it holds for the $d = 2$ case:

$$v_{\mathrm{D}}^{(\infty)}(f \downarrow f_{\mathrm{c}}^-) \simeq \frac{1}{2}(v_{\mathrm{L}}/v_{\mathrm{A}})^{1/2}\mu_0(f - f_{\mathrm{c}}^-) \sim f - f_{\mathrm{c}}^-\,. \tag{S18}$$

The critical laws in Eqs. (S13) and (S18) can be summarized for $d = 2, 3$ as

$$v_{\mathrm{D}}^{(\infty)}(f \downarrow f_{\mathrm{c}}^-) \simeq \frac{1}{d}\big[(d-1)v_{\mathrm{L}}v_{\mathrm{A}}\big]^{1/2}\,\big[\mu_0(f - f_{\mathrm{c}}^-)/v_{\mathrm{A}}\big]^{d/2}\,. \tag{S19}$$

Figure S2 corroborates this analytic result, which coincides asymptotically ($f \downarrow f_{\mathrm{c}}^-$) with the data for $v_{\mathrm{D}}^{(\infty)}(f)$ from the quadrature of the $\boldsymbol{u}$-average [Eq. (S8) for $d = 3$, Eq. (S14) for $d = 2$].

Dispersion coefficient

Concerning the dispersion of the trajectories, we note first that the sequence of reorientations yields, in full analogy to the particle collisions in a dilute gas, for the velocity autocorrelation function:

$$\begin{aligned} Z(t) &= \langle [v_{\mathrm{D}}(f;\vartheta(t)) - v_{\mathrm{D}}^{(\infty)}(f)]\,[v_{\mathrm{D}}(f;\vartheta(0)) - v_{\mathrm{D}}^{(\infty)}(f)]\rangle \\ &= \mathrm{Var}[v_{\mathrm{D}}(f;\vartheta_i)]_{\boldsymbol{u}}\,\mathrm{e}^{-t/\tau_{\mathrm{R}}}\,, \end{aligned} \tag{S20}$$

taking into account that $\langle v_{\mathrm{D}}(f;\vartheta_i)\rangle_{\boldsymbol{u}} = v_{\mathrm{D}}^{(\infty)}(f)$ may not be zero. The factor $\mathrm{e}^{-t/\tau_{\mathrm{R}}}$ is simply the probability that no "collision" has occurred in the time interval $[0, t]$. The effective diffusion coefficient then follows from the Green–Kubo relation:

$$\begin{aligned} D_{\mathrm{eff}}(f) &= \int_0^\infty Z(t)\,\mathrm{d}t = \mathrm{Var}[v_{\mathrm{D}}(f;\vartheta_i)]_{\boldsymbol{u}}\tau_{\mathrm{R}} \\ &= \big(\langle v_{\mathrm{D}}(f;\vartheta_i)^2\rangle_{\boldsymbol{u}} - v_{\mathrm{D}}^{(\infty)}(f)^2\big)\tau_{\mathrm{R}}\,. \end{aligned} \tag{S21}$$

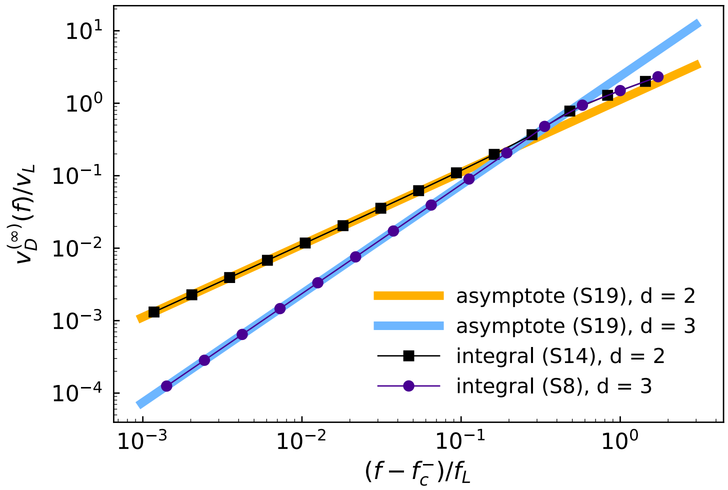

FIG. S2. Critical behavior of the drift velocity $v_{\mathrm{D}}^{(\infty)}(f)$ in the lazy-wobbling limit ($\tau_{\mathrm{R}} \to \infty$) as function of the distance to the critical point, $\varepsilon = (f - f_{\mathrm{c}}^-)/f_{\mathrm{L}}$, evaluated for $v_{\mathrm{A}}/v_{\mathrm{L}} = 0.2$ and for rotational motion in $d = 2$ and $d = 3$ dimensions. Solid lines show the analytic prediction for both cases [Eq. (S19)] and symbols denote numerical results from the quadrature of the orientational $\boldsymbol{u}$-average given in Eq. (S14) for $d = 2$ (squares) and Eq. (S8) for $d = 3$ (circles); the latter agree also with the explicit expression in Eq. (S11).

It remains to compute the second moment, $\langle v_{\mathrm{D}}(f;\vartheta_i)^2\rangle_{\boldsymbol{u}}$. The same arguments apply that have led to Eq. (S9) for the first moment in the case $d = 3$. Therefore:

$$\begin{aligned}\langle v_{\mathrm{D}}(f;\vartheta_i)^2\rangle_{\boldsymbol{u}} &= \frac{v_{\mathrm{L}}^2}{2}\int_{-1}^{1} s(f/f_{\mathrm{L}} + (v_{\mathrm{A}}/v_{\mathrm{L}})u_x)^2 \mathrm{d}u_x \\ &= \frac{v_{\mathrm{L}}^3}{2v_{\mathrm{A}}}\int\limits_{\max(y_-,1)}^{\max(y_+,1)} \left(y^2-1\right)\mathrm{d}y \end{aligned} \tag{S22}$$

Introducing $\tilde{w}(y) := \int_1^y s(y')^2\,\mathrm{d}y' = \frac{1}{3}\left(y^3-1\right) + 1 - y$ and $\tilde{w}_\pm(f/f_{\mathrm{L}}) = \tilde{w}(y_\pm)$ and noting that $\tilde{w}(1) = 0$, it follows

$$\langle v_{\mathrm{D}}(f;\vartheta_i)^2\rangle_{\boldsymbol{u}} = \frac{v_{\mathrm{L}}^3}{2v_{\mathrm{A}}}\begin{cases} 0, & f \leqslant f_{\mathrm{c}}^-, \\ \tilde{w}_+(f/f_{\mathrm{L}}), & f_{\mathrm{c}}^- < f < f_{\mathrm{c}}^+, \\ \tilde{w}_+(f/f_{\mathrm{L}}) - \tilde{w}_-(f/f_{\mathrm{L}}), & f \geqslant f_{\mathrm{c}}^+, \end{cases} \tag{S23}$$

which can be rewritten in the form

$$\langle v_{\mathrm{D}}(f;\vartheta_i)^2\rangle_{\boldsymbol{u}} = v_{\mathrm{L}}^2 \times \begin{cases} 0, & f \leqslant f_{\mathrm{c}}^-, \\ \dfrac{v_{\mathrm{L}}/v_{\mathrm{A}}}{6f_{\mathrm{L}}^3}(f-f_{\mathrm{c}}^-)^2(f+f_{\mathrm{c}}^+ + f_{\mathrm{L}}), & f_{\mathrm{c}}^- < f < f_{\mathrm{c}}^+, \\ (f/f_{\mathrm{L}})^2 + \dfrac{1}{3}(v_{\mathrm{A}}/v_{\mathrm{L}})^2 - 1, & f \geqslant f_{\mathrm{c}}^+. \end{cases} \tag{S24}$$

The dispersion coefficient $D_{\mathrm{eff}}(f)$ is obtained by inserting Eqs. (S11) and (S24) into Eq. (S21), and its behavior is exemplarily shown in Fig. 1(f) of the main text (orange line).